Fusion Engineering and Design 170 (2021) 112526

Contents lists available at ScienceDirect

Fusion Engineering and Design

journal homepage: www.elsevier.com/locate/fusengdes

Integrated Control and Actuator Management Strategies for Internal Inductance and Normalized Beta Regulation

A. Pajares *, E. Schuster

Department of Mechanical Engineering and Mechanics, Lehigh University, Bethlehem, PA 18015, USA

ARTICLE INFO

Keywords:
Plasma control
Integrated control
Internal inductance control
Beta control
Supervisory control

ABSTRACT

An integrated-control architecture for simultaneous regulation of the plasma internal inductance and normalized beta has been designed and tested in simulations using COTSIM (Control-Oriented Transport SIMulator). As present-day tokamaks evolve into nuclear-fusion reactors capable of producing net energy, a significant control-engineering challenge must be solved: regulating a wide variety of plasma variables, often simultaneously, by employing only a reduced number of actuators. As a contribution towards this objective, the present work tackles the problem of controlling the plasma internal inductance, which is a proxy for the broadness of the current-density profile, simultaneously with the plasma normalized beta. Based on zero-dimensional, control-oriented models of the plasma dynamics, individual Lyapunov-theory-based controllers for the internal inductance and normalized beta have been developed. These controllers are integrated by means of an actuator manager that decides, in real time, how the available actuators are utilized in order to fulfill as many control objectives as possible. In addition, the actuator manager is designed to achieve a particular performance metric defined by the control engineer. This metric could be, for example, prioritizing a particular control task over the others and/or minimizing the use of a particular actuator during certain phases of the plasma discharge. Using COTSIM, which includes one-dimensional models of the plasma current-density and electron-temperature dynamics, the performance of the integrated-control framework has been tested in a steady-state scenario for the DIII-D tokamak. These simulation results yield illustrative insights into the plasma current-density and electron-temperature controllability with the current actuation capabilities in DIII-D. Moreover, these simulations show that the way in which the different actuators are employed during the discharge (based on the choice of the aforementioned actuator-manager performance metric) highly determines the value of internal inductance and normalized beta achieved in steady-state conditions, and therefore, the final current-profile shape.

1. Introduction

In tokamaks, there is a multitude of plasma variables for which different degrees of regulation are needed. For example, accurate regulation of the current and pressure profiles can play a critical role, particularly in Advanced Tokamak (AT) scenarios [1], in achieving a particular steady-state evolution with high pressure and high non-inductive fraction. However, controlling several profiles at numerous spatial locations can be challenging and often not even feasible. Fortunately, regulating global variables related to those profiles may sometime suffice to meet the required control goals. For instance, the line-average electron density, $\bar{n}_e$, the internal inductance, L_i, and the normalized beta, β_N, can be used as proxies for the electron density, current, and pressure profiles, respectively. Despite the multitude of control tasks that must be carried out in a reactor-grade tokamak [2], only a finite number of shared actuators will be available to carry out the aforementioned control of multiple global variables. As an example, the electron-cyclotron (EC) system can heat the plasma and drive current, so it can be employed both synchronously and asynchronously during control tasks such as current-profile control, neoclassical tearing mode (NTM) suppression, or burn control. Moreover, actuator availability may change during operation, e.g., as a result of trips triggered by potentially unsafe actuator conditions. Integrated architectures with actuator management capabilities will be required in future tokamaks to ensure safe and efficient operation.

In the present work, simultaneous control of L_i and β_N is considered, together with actuator management. Previous work on L_i control using ohmic coil, PF coils, and non-inductive current sources can be found in

* Corresponding author.
E-mail address: andres.pajares@lehigh.edu (A. Pajares).

https://doi.org/10.1016/j.fusengdes.2021.112526
Received 25 November 2020; Received in revised form 17 March 2021; Accepted 21 March 2021
Available online 8 April 2021

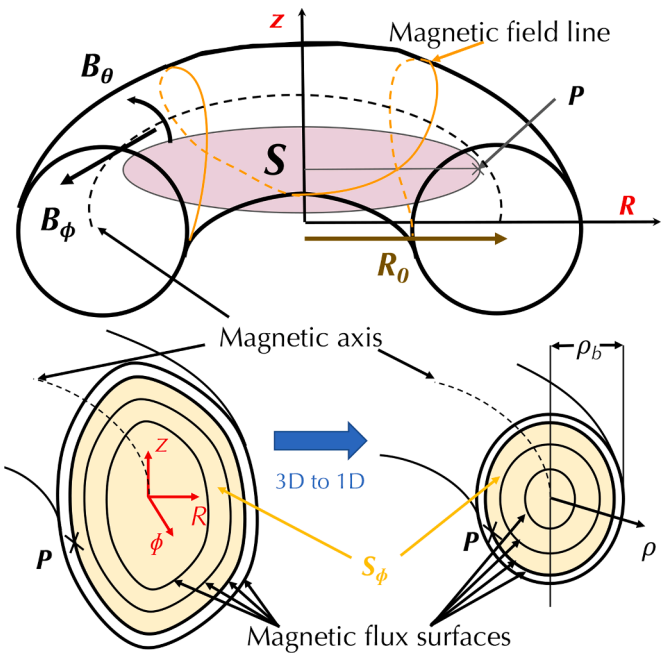

Fig. 1. Magnetic geometry and spatial-coordinate transformation employed in this work. The model dimensionality is reduced from 3D to 1D due to the assumptions of toroidal symmetry and nested flux surfaces.

[3–5], whereas work on L_i regulation using only ohmic and/or PF coils can be found in [6–8]. Some of this previous work employs non-model based, linear techniques (e.g., [3]), but model-based, nonlinear-control techniques have also been utilized (e.g., [4]). In recent years, the actuator management problem has received increasing attention. Previous work includes [9,10], which propose algorithms that minimize a cost function over a finite set of actuator-allocation options, or [11], where a mixed-integer algorithm is proposed.

The model-based, nonlinear-control scheme proposed in this work is composed of three elements: (1) L_i controller, (2) β_N controller, and (3) actuator manager. The actuators considered are neutral beam injection (NBI) and EC heating and current drive (H&CD), i.e., only non-inductive current sources. The ohmic and PF coils are not considered in this work because of their coupling with plasma shape and I_p control. The controllers for L_i and β_N are synthesized by means of Lyapunov techniques [12]. These controllers compute requests related to the non-inductive current and auxiliary heating power that ensure L_i and β_N regulation, respectively. Based on the controller requests, as well as real-time information on actuator availability, the actuator manager solves an optimization problem in real time (previous efforts along this line can be found in [13]) to compute the requests that are sent to the actuators.

This paper is organized as follows. In Section 2, the model employed for control synthesis is introduced. In Section 3, the elements composing the control scheme are synthesized: the nonlinear, Lyapunov-based controllers (Sections 3.1 and 3.2), and the actuator manager (Section 3.3). In Section 4, simulation results using the Control-Oriented Transport SIMulator (COTSIM) are presented. Finally, a conclusion and possible future work are presented in Section 5.

2. Modeling for Control Synthesis

2.1. Modeling of the Internal Inductance Dynamics

The L_i model is based on the magnetic diffusion equation (MDE) [14]. The MDE determines the dynamics of the poloidal stream function, ψ. At a point P, ψ is given by $\psi \triangleq \frac{1}{2\pi}\int_S \vec{B}_\theta \cdot \vec{dS}$, where B_θ is the poloidal magnetic field, and S is the surface that is perpendicular to the z axis and enclosed by the toroidal circumference passing through the point P, as depicted in Fig. 1. By exploiting this relationship between $\vec{B}_\theta$ and ψ, the magnetic field, $\vec{B}$, can be expressed as

$$\vec{B} = B_\phi \vec{\phi} + \vec{B}_\theta = B_\phi \vec{\phi} - \frac{1}{R}(\nabla\psi \times \vec{\phi}), \tag{1}$$

where B_ϕ is the toroidal magnetic field, R is the radial coordinate, and $\vec{\phi}$ is the toroidal-direction unit vector (see Fig. 1).

A magnetic-flux surface is defined by points with constant ψ, and they form nested surfaces around the magnetic axis under ideal magnetohydrodynamic (MHD) conditions. The mean-effective minor radius, ρ, is the spatial coordinate employed to describe the dynamics of L_i. It is defined as $\rho \triangleq \sqrt{\Phi/(\pi B_{\phi,0})}$, where $\Phi \triangleq \int_{S_\phi} B_\phi dS_\phi$ is the toroidal flux, S_ϕ is the toroidal surface perpendicular to the ϕ axis and enclosed by a magnetic-flux surface as depicted in Fig. 1, and $B_{\phi,0}$ is the vacuum toroidal field at the magnetic axis. The mean-effective minor radius can be normalized by ρ_b, which is the value of ρ at the last closed magnetic-flux surface, so that $\widehat{\rho} \triangleq \rho/\rho_b$. The MDE model is closed by means of physics-based, control-oriented models [15] for the plasma resistivity, η, electron density, n_e, electron temperature, T_e, auxiliary-source-driven current, j_{aux} (from NBI and EC in this work), and bootstrap current, j_{BS}. Using the control-oriented models, the MDE can be written as

$$\dot{\psi} = (f_1\psi' + f_2\psi'')u_\eta + \sum_i^{N_{NBI}} f_{NBI,i}u_{NBI,i} + f_{EC}u_{EC} + \frac{f_{BS}}{\psi'}u_{BS}, \tag{2}$$

where $()' \triangleq \partial()/\partial\widehat{\rho}$, $\dot{()} \triangleq \partial()/\partial t$, $f_1(\widehat{\rho})$ and $f_2(\widehat{\rho})$ characterize the spatial distribution of the poloidal-flux diffusion, $f_{NBI,i}(\widehat{\rho})$ are spatial profiles related to the NBI current (for $i = 1, \ldots, N_{NBI}$, where N_{NBI} is the total number of NBIs), $f_{EC}(\widehat{\rho})$ is a spatial profile related to the EC current, $f_{BS}(\widehat{\rho})$ characterizes the spatial distribution of the bootstrap current, and $u_{(\cdot)}(t)$ are virtual inputs given by

$$u_\eta = \left(I_p^\gamma P_{tot}^\epsilon \overline{n}_e^\zeta\right)^{-3/2}, \quad u_{BS} = \left(I_p^\gamma P_{tot}^\epsilon \overline{n}_e^\zeta\right)^{-1/2} \overline{n}_e, \tag{3}$$

$$u_{NBI,i} = \left(I_p^\gamma P_{tot}^\epsilon \overline{n}_e^\zeta\right)^{-3/2+\delta_{NBI,i}} \overline{n}_e^{-1} P_{NBI,i} \tag{4}$$

$$u_{EC} = \left(I_p^\gamma P_{tot}^\epsilon \overline{n}_e^\zeta\right)^{-3/2+\delta_{EC}} \overline{n}_e^{-1} P_{EC}, \tag{5}$$

where I_p is the total plasma current, $P_{tot} \triangleq \sum_i P_{NBI,i} + P_{EC}$ is the total injected power (where $P_{NBI,i}$ is the power injected by the i-th NBI and P_{EC} is the EC power), $\overline{n}_e$ is the line-average electron density, and $\gamma, \epsilon, \zeta, \delta_{NBI,i}$, and δ_{EC} are model constants. The controllable inputs (actuators) considered in this work are $P_{NBI,i}$ and P_{EC}. Both I_p and $\overline{n}_e$ are considered as non-controllable inputs to the model. The boundary conditions for the MDE (2) are given by

$$\psi'(\widehat{\rho}=0) = 0, \quad \psi'(\widehat{\rho}=1) = -k_{I_p} I_p, \tag{6}$$

where k_{I_p} is a model parameter depending on the equilibrium.

By defining the poloidal-flux gradient, θ, as

$$\theta \triangleq \frac{\partial\psi}{\partial\widehat{\rho}}, \tag{7}$$

and taking derivative with respect to $\widehat{\rho}$, the MDE (2) can be rewritten as

$$\begin{aligned}\dot{\theta} = {} & (h_0\theta + h_1\theta' + h_2\theta'')u_\eta + \sum h_{NBI,i}u_{NBI,i} \\ & + h_{EC}u_{EC} + \left(\frac{1}{\theta}h_{BS,1} - \frac{\theta'}{\theta^2}h_{BS,2}\right)u_{BS},\end{aligned} \tag{8}$$

where $h_{(\cdot)}$ are obtained from $f_{(\cdot)}$ by applying the chain rule.

The plasma internal inductance, L_i, is defined as

$$L_i \triangleq \frac{2W_\theta}{I_p^2}, \tag{9}$$

where W_θ is the energy enclosed by $\vec{B}_\theta$, and is given by

$$W_\theta = \frac{1}{2\mu_0}\int_V B_\theta^2 dV, \tag{10}$$

where μ_0 is the vacuum permeability, and V is the plasma volume. Using (1), (7), and $\nabla\psi = (\partial\psi/\partial\widehat{\rho})\nabla\widehat{\rho}$, it is found that

$$B_\theta^2 = \frac{\theta^2(\nabla\widehat{\rho})^2}{R^2}, \tag{11}$$

so (10) becomes

$$W_\theta = \frac{1}{2\mu_0}\int_V \frac{\theta^2(\nabla\widehat{\rho})^2}{R^2} dV \approx \frac{1}{2\mu_0}\int_0^1 \theta^2 \frac{G}{(\rho_b R_0)^2} V' d\widehat{\rho}, \tag{12}$$

where $(\nabla\widehat{\rho})^2/R^2$ has been approximated by its flux-surface average, denoted by $\langle(\nabla\widehat{\rho})^2/R^2\rangle$, and the definitions $G \triangleq \langle R_0^2(\nabla\rho)^2/R^2\rangle$ and $V' \triangleq \partial V/\partial\widehat{\rho}$ have been employed, where R_0 is the major radius. Using the expression for W_θ in (12), the definition for L_i given in (9) becomes

$$L_i = \frac{1}{\mu_0 R_0^2 \rho_b^2 I_p^2}\int_0^1 \theta^2 G V' d\widehat{\rho}. \tag{13}$$

2.2. Modeling of the Normalized Beta Dynamics

The normalized beta, β_N, is defined as

$$\beta_N \triangleq \beta_t[\%] a B_{\phi,0}/I_p, \tag{14}$$

where a is the plasma minor radius, and β_t is the toroidal beta, which is given by

$$\beta_t \triangleq 2\mu_0\left(\frac{1}{V}\int_V p dV\right)\Big/ B_{\phi,0}^2 \approx \frac{4}{3}\mu_0 W \Big/ \left(V B_{\phi,0}^2\right), \tag{15}$$

where p is the plasma pressure, and $W = \frac{3}{2}p$ is the thermal stored energy. Because I_p is considered as a non-controllable input, it can be seen from (14)-(15) that β_N can be controlled by regulating W in this case. A 0D energy balance is employed to model the dynamics of W,

$$\frac{dW}{dt} = -\frac{W}{\tau_E(P_{tot})} + P_{tot}, \tag{16}$$

where τ_E is the energy confinement time, which is modeled using the ITERH-98P(y,2) scaling,

$$\tau_E = 0.0562 H_H I_p^{0.93} B_{\phi,0}^{0.15} a^{0.58} R_0^{1.39} \kappa^{0.78} A_{eff}^{0.19} \overline{n}_{e,19}^{0.41} P_{tot}^{-0.69}, \tag{17}$$

where H_H is the so-called H-factor, κ is the plasma elongation, A_{eff} is the effective plasma mass, and $\overline{n}_{e,19}$ is the line-average electron density in $10^{19}\mathrm{m}^{-3}$. Because I_p and $\overline{n}_e$ are non-controllable inputs, τ_E can be modified for control purposes only by means of P_{tot}.

3. Control Synthesis

3.1. Control of L_i via Lyapunov Techniques

The MDE in (8) is a partial differential equation that can be reduced to a set of ordinary differential equations by using the finite differences method over the spatial domain. By using $N+1$ nodes equally distributed over $\widehat{\rho} = [0, 1]$, a discretization step $\Delta\widehat{\rho} = 1/N$ is employed. Thus, (6)-(8) become

$$\dot{\widehat{\theta}} = H(\widehat{\theta}, I_p)u, \tag{18}$$

where $\widehat{\theta} = [\theta(\Delta\widehat{\rho}), \theta(2\Delta\widehat{\rho}), ..., \theta(1-\Delta\widehat{\rho})]^T$ is a vector with the values of θ at the interior discretization nodes, $u = [u_\eta, u_{NBI,1}, ..., u_{NBI,N_{NBI}}, u_{EC}, u_{BS}]^T$ is a vector with the virtual inputs (3)-(5), and $H(\widehat{\theta}, I_p) \in \mathbb{R}^{(N-1)\times(N_{NBI}+3)}$ is a matrix which is a function of $h_{(\cdot)}$. In addition, L_i in (13) can be approximated, using the trapezoid rule over the same $N+1$ nodes, as

$$L_i \approx \frac{\left[\sum_{i=1}^{i=N-1}(\theta^2 GV')_{i\Delta\widehat{\rho}} + \frac{1}{2}k_{I_p}^2 I_p^2 G(1)V'(1)\right]}{\mu_0 R_0^2 \rho_b^2 I_p^2}, \tag{19}$$

where (6) has been employed. It can be noted that, because I_p is a non-controllable input, and the ohmic and PF coils are not considered as actuators (so ρ_b, G, V, and k_{I_p} cannot be directly controlled), control of L_i can only be achieved by controlling $\widehat{\theta}$.

For convenience, a normalized version of L_i can be defined,

$$L_i^* \triangleq L_i\mu_0 R_0^2 \rho_b^2 I_p^2 - \frac{1}{2}k_{I_p}^2 I_p^2 G(1)V'(1) = \sum_{i=1}^{i=N-1}\left(\theta^2 GV'\right)_{i\Delta\widehat{\rho}}, \tag{20}$$

and taking time derivative in (20), a dynamics equation is obtained,

$$\frac{dL_i^*}{dt} = \sum_{i=1}^{i=N-1} 2\left(\theta GV'\frac{d\theta}{dt}\right)_{i\Delta\widehat{\rho}} = 2(\widehat{\theta}^*)^T H(\widehat{\theta}, I_p)u, \tag{21}$$

where $\widehat{\theta}^* \triangleq [(\theta GV')_{\Delta\widehat{\rho}}, ..., (\theta GV')_{1-\Delta\widehat{\rho}}]^T$, and (18) has been employed. By setting the right-hand side of (21) as

$$2(\widehat{\theta}^*)^T H(\widehat{\theta}, I_p)u = -K_P^{L_i}\widetilde{L}_i^* - K_I^{L_i}\int_0^t \widetilde{L}_i^* dt + \frac{d\overline{L}_i^*}{dt}, \tag{22}$$

where $K_P^{L_i}, K_I^{L_i} > 0$ are design parameters, $\widetilde{L}_i^* \triangleq L_i^* - \overline{L}_i^*$ is the error variable for L_i^*, and $\overline{L}_i^*$ is the target for L_i^*, it can be ensured that the L_i^* evolution is asymptotically stable (see Appendix A). For example, taking $x_1 \triangleq \widetilde{L}_i^*$, $x_2 \triangleq \int_0^t \widetilde{L}_i^* dt$, and a Lyapunov function $V_{L_i} = \frac{1}{2}x_1^2 + \frac{1}{2}K_I^{L_i}x_2^2$, then $\dot{V}_{L_i} = -K_P^{L_i}x_1^2$. Thus, $V_{L_i} \geq 0$ and $\dot{V}_{L_i} \leq 0$. Also, it can be appreciated that $\dot{V}_{L_i} < 0$ for all (x_1, x_2) different from the origin except for points within the subset $S = \{(x_1, x_2) \in \mathbb{R}^2 \,|\, x_1 \equiv 0\}$. However, no point can stay identically in S ($x_1 \equiv 0$) other than the origin ($x_1 \equiv x_2 \equiv 0$), as it can be demonstrated from equations (21)-(22). Using La Salle's invariance principle, it can be concluded that the L_i^* dynamics is asymptotically stable. It must be noted that (22) is a constraint for the controllable inputs (namely, $P_{NBI,i}$ ($i = 1$, ..., N_{NBI}) and P_{EC}) because u is a function of them (see equations (3)-(5)).

3.2. Control of β_N via Lyapunov Techniques

If the right-hand side of (16) is set as

$$-\frac{W}{\tau_E(P_{tot})} + P_{tot} = -K_P^W\widetilde{W} - K_I^W\int_0^t \widetilde{W} dt + \frac{d\overline{W}}{dt}, \tag{23}$$

where $K_P^W, K_I^W > 0$ are design parameters, $\widetilde{W} \triangleq W - \overline{W}$ is the error variable for W, and $\overline{W}$ is the target for W, then it can be ensured that the W evolution is asymptotically stable. To demonstrate this, $V_W = \frac{1}{2}x_1^2 + \frac{1}{2}K_I^W x_2^2$ with $x_1 \triangleq \widetilde{W}$ and $x_2 \triangleq \int_0^t \widetilde{W} dt$ is used as Lyapunov function, which yields $\dot{V}_W = -K_P^W x_1$. Using the same arguments as in Section 3.1, asymptotical stability of the W dynamics is proved by La Salle's invariance principle (see Appendix A). It must be noted that (23) is a constraint for the controllable inputs because $P_{tot} \triangleq \sum_i P_{NBI,i} + P_{EC}$.

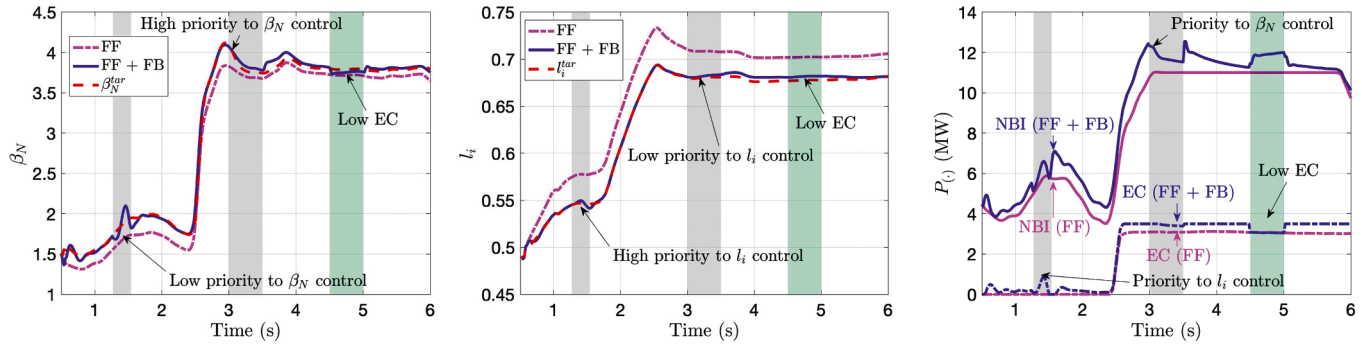

Fig. 2. Time evolution for β_N, L_i, $P_{NBI} \triangleq \sum P_{NBI,i}$, and P_{EC} in FF (magenta), FF + FB (blue), and target (red) simulations. The grey shaded areas denote periods of time when either β_N or L_i control are prioritized, whereas the green shaded areas denote periods of time when EC use is penalized.

3.3. Actuator Management via Real-Time Optimization

The feedback laws (22) and (23) represent two constraints for $N_{NBI}+1$ controllable inputs, i.e., $P_{NBI,i}$ $(i=1,\ldots,N_{NBI})$ and P_{EC}. Therefore, in general, (22) and (23) do not univocally determine the controllable inputs. In addition, while it is desired to fulfill the control constraints (22) and (23) as closely as possible, actuator limits exist that may prevent it. In some occasions, it might not be possible to fulfill both control requests at the same time (due to unreachable targets and/or limited actuation availability), or it may be desirable to control one of the plasma variables more tightly than the other. The control constraints (22) and (23) can be rewritten as

$$2(\widehat{\theta}^*)^T H(\widehat{\theta}, I_p)u + s_1 = -K_P^{L_i}\widetilde{L}_i^* - K_I^{L_i}\int_0^t \widetilde{L}_i^* dt + \frac{d\widetilde{L}_i^*}{dt}, \tag{24}$$

$$-\frac{W}{\tau_E(P_{tot})} + P_{tot} + s_2 = -K_P^W \widetilde{W} - K_I^W \int_0^t \widetilde{W} dt + \frac{d\widetilde{W}}{dt}, \tag{25}$$

where $s_{(\cdot)}$ are slack variables that characterize whether the control constraints are satisfied. When $s_{(\cdot)}$ are zero, asymptotical stability is ensured as demonstrated in Sections (3.1) and (3.2). For the case when $s_{(\cdot)}$ are different from zero, consider the regions $|\widetilde{L}_i^*| \geq |s_1|/k_1$ and $|\widetilde{W}| \geq |s_2|/k_2$, with $k_1 < K_P^{L_i}$ and $k_2 < K_P^W$. In such regions, $\dot{V}_{L_i} \leq -(K_P^{L_i} - k_1)x_1^2 \triangleq -k_1^* x_1^2$ and $\dot{V}_W \leq -(K_P^W - k_2)\widetilde{W}^2 = -k_2^*\widetilde{W}^2$, respectively, with $k_1^* \triangleq K_P^{L_i} - k_1 > 0$ and $k_2 \triangleq K_P^W - k_2 > 0$. Therefore, the L_i^* and W dynamics are input-to-state stable with respect to s_1 and s_2, respectively (see Appendix B), and bounded as $|\widetilde{L}_i^*| \leq \sup_{0\leq\tau\leq t}(s_1(\tau))/k_1$ and $|\widetilde{W}| \leq \sup_{0\leq\tau\leq t}(s_2(\tau))/k_2$. It can be noted that the higher $K_P^{L_i}$ and K_P^W are, the higher k_1 and k_2 can be taken, making the bounds over $|\widetilde{L}_i^*|$ and $|\widetilde{W}|$ tighter. Also, the smaller s_1 and s_2 are, the tighter the bounds for $|\widetilde{L}_i^*|$ and $|\widetilde{W}|$ become.

The controllable inputs are obtained by means of an actuator manager that solves an optimization problem in real time, i.e.

$$\min_{P_{NBI,i}, P_{EC}} s^T Q s + P_{aux}^T R P_{aux}, \tag{26}$$

$$\text{subject to} \quad L_i \text{and} \beta_N \text{control constraints (24) and (25)} \tag{27}$$

$$\left[P_{NBI,1}, \ldots, P_{NBI,N_{NBI}}, P_{EC}\right] \subset P_{limits}, \tag{28}$$

where $s = [s_1, s_2]^T$, Q and R are design matrices, and P_{lim} is the set of feasible controllable inputs. By changing the weights in Q, the control tasks can be prioritized in real-time, whereas changes to the weights in R allow for prioritizing or penalizing the use of particular actuators.

4. One-Dimensional Simulations using COTSIM

The control scheme is tested using COTSIM, a control-oriented code that evolves 1D models for the dynamics of L_i and β_N based on the MDE and heat-transport equations. A DIII-D steady-state, high-q_{min} scenario is used where on-axis NBI, off-axis NBI, and EC are employed. First, a feedforward (FF) simulation is carried out using the experimental inputs from shot 172538. Reachable targets different from the evolutions during the FF simulation are set for β_N and L_i (denoted by β_N^{tar} and L_i^{tar}, respectively). Finally, a FF + feedback (FB) simulation is executed in which the controller tries to drive β_N and L_i toward β_N^{tar} and L_i^{tar}, respectively. Also, changes to the actuator-manager matrices Q and R are introduced during the FF + FB simulation, so β_N control is prioritized in $t = [1.25, 1.5]$ s, L_i control is prioritized in $t = [3, 3.5]$ s, and EC use is penalized in $t = [4.5, 5]$ s.

Fig. 2 shows the β_N and L_i evolutions during the FF and FF + FB simulations, the targets, and the FF and FF + FB actuator trajectories for $P_{NBI} \triangleq \sum_i P_{NBI,i}$ and P_{EC}. It can be observed that successful regulation of both β_N and L_i is achieved in FF + FB. The periods of time during which β_N or L_i are prioritized correspond to specially challenging changes in β_N^{tar} and L_i^{tar}, respectively. The L_i control performance is worsened when β_N control is prioritized, and vice versa, although the actuator manager ensures that both evolutions remain close to their targets. When EC use is penalized, the actuator manager increases P_{NBI} to compensate for the reduction in P_{EC}, with the final goal of regulating both β_N and L_i despite this change in actuator usage. Although L_i converges towards its target more slowly than β_N, convergence is achieved before the end of the simulation.

5. Conclusion and Possible Future Work

The nonlinear, Lyapunov-based controllers proposed in this work for $\beta_N + L_i$ regulation show good performance and robustness in 1D simulations, despite being synthesized from 0D models. The capabilities of the real-time, optimization-based actuator manager to prioritize control tasks and actuator usage have also been demonstrated. Future work may include both simulation testing by coupling the transport equations with a 2D equilibrium solver and experimental testing in DIII-D.

Declaration of Competing Interest

The authors declare that they have no known competing financial interests or personal relationships that could have appeared to influence the work reported in this paper.

Acknowledgments

This material is based upon work supported by the U.S. Department of Energy, Office of Science, Office of Fusion Energy under Award Numbers DE-SC0010661 and DE-FC02-04ER54698.

Appendix A. Asymptotical Stability using Lyapunov Theory and La Salle's Invariance Principle

Consider a nonlinear system $\dot{x} = f(x)$ in a domain $D \subset \mathbb{R}^n$. Assume $x = 0$ is an equilibrium point contained in D. Then, if a continuously differentiable function $V : D \rightarrow \mathbb{R}$ can be found such that

$$V(x) \geq 0, \quad \dot{V}(x) \leq 0, \tag{A.1}$$

for all $x \in D$, then $x = 0$ is a stable equilibrium. In addition, if $\dot{V}(x) < 0$, then $x = 0$ is asymptotically stable.

When $\dot{V}(x) < 0$ is not fulfilled, La Salle's invariance principle can be employed to demonstrate asymptotical stability. It states that, under the conditions given in (A.1), if no solution to $\dot{x} = f(x)$ can stay identically in S other than the trivial solution, where $S = \{x \in D \,\big|\, \dot{V}(x) = 0\}$, then the equilibrium $x = 0$ is asymptotically stable. More details can be found in [12].

Appendix B. Input-to-state Stability via Lyapunov Theory

Consider a nonlinear system $\dot{x} = f(x, u)$, where f is defined in the domain $[D_1, D_2]$ ($D_1 \subset \mathbb{R}^n$, $D_2 \subset \mathbb{R}^m$), x is the state vector, and u is the input vector. This system is said to be input-to-state stable if, for any initial state x_0 and bounded input u, the state x fulfills

$$\| x \| \leq \gamma\left(\sup_{0 \leq \tau \leq t}(u)\right) + \beta(\|x_0\|, t), \tag{B.1}$$

where γ is a class K function (i.e., (i) γ is strictly increasing, and (ii) $\gamma(0) = 0$), sup denotes the supreme, and β is a class KL function (i.e., (i) it is class K with respect to its first argument, (ii) it is decreasing with respect to its second argument, and (iii) $\lim_{y \rightarrow \infty} \beta(x, y) = 0$).

Assume that a continuously differentiable function $V : D_1 \rightarrow \mathbb{R}$ can be found such that

$$\alpha_2(\| x \|) \geq V(x) \geq \alpha_1(\| x \|), \tag{B.2}$$

$$\dot{V}(x, u) \leq -W_3(x), \tag{B.3}$$

where α_i are class K_∞ functions of x (i.e., (i) α_i is strictly increasing, (ii) $\alpha_i(0) = 0$, and (iii) $\lim_{x \rightarrow \infty} \alpha_i(x) = \infty$). Condition (B.2) is fulfilled for all $x \in D_1$ and $u \in D_2$, whereas condition (B.3) is fulfilled for all $\| x \| \geq \rho(\| u \|) > 0$ within D_1, where ρ is a class K function. When all previous conditions are satisfied, the system is input-to-state stable with $\gamma = \alpha_1 \circ \alpha_2 \circ \rho$, where $\circ$ denotes a function product. More details can be found in [12].

References

[1] E. Joffrin, Advanced Tokamak Scenario Developments for the Next Step, Plasma Physics and Controlled Fusion 49 (B629) (2007).
[2] D. Humphreys, et al., Integrated Plasma Control in DIII-D, Fusion Science and Technology 48 (2) (2005) 1249–1263.
[3] T. Wijnands, et al., Feedback Control of the Current Profile on Tore Supra, Nucl. Fusion 37 (6) (1997) 777.
[4] J. Romero, et al., Tokamak Plasma Inductance Control at JET, 36th EPS Conference on Plasma Physics, Sofia, Bulgaria 33E (2009) P–5.177.
[5] F. Felici, et al., Enhancing Current Density Profile Control in Tokamak Experiments using Iterative Learning Control. 54th IEEE CDC, 2018.
[6] J.A. Romero, et al., Current Profile Control Using the Ohmic Heating Coil in TCV. 24th IAEA FEC, San Diego, USA, 2012.
[7] I. Garrido, et al., Robust Sliding Mode Control for Tokamaks, Mathematical Problems in Engineering (ID 341405) (2012) 14.
[8] I. Garrido, et al., Internal Inductance Predictive Control for Tokamaks, World Automation Congress, Waikoloa, USA (2014) pp.628–633.
[9] C.J. Rapson, et al., Experiments on actuator management and integrated control at ASDEX Upgrade, Fusion Eng. Des. 123 (2017) 603–606.
[10] N.M. Vu, et al., Tokamak-agnostic actuator management for multi-task integrated control with application to TCV and ITER, Fusion Eng. Des. 147 (111260) (2019).
[11] E. Maljaars, et al., Actuator allocation for integrated control in tokamaks: architectural design and a mixed-integer programming algorithm, Fusion Eng. Des. 122 (2017) 94–112.
[12] H. Khalil, Nonlinear Systems, 3rd, Prentice Hall, NJ, 2001.
[13] A. Pajares, E. Schuster, Actuator Management via Real-time Optimization for Integrated Control in Tokamaks. 46th EPS CPP, 2019.
[14] F.L. Hinton, R.D. Hazeltine, Theory of plasma transport in toroidal confinement systems, Reviews of Modern Physics 48 (2) (1976) 239–308.
[15] J. Barton, W. Shi, et al., Physics-based control-oriented modeling of the safety factor profile dynamics in high performance tokamak plasmas. 52nd IEEE CDC, 2013.